

Low DNA and high BSA binding affinity of cationic ruthenium(II) organometallic featuring pyridine and 2'-hydroxychalcone ligands

Adnan Zahirović^a, Sunčica Roca^b, Emira Kahrović^a, Aleksandar Višnjevac^{c,*}

^aLaboratory for Inorganic and Bioinorganic Chemistry, Department of Chemistry, Faculty of Science, University of Sarajevo, 71 000 Sarajevo, Bosnia and Herzegovina

^bNMR Centre, Ruđer Bošković Institute, 10 000 Zagreb, Croatia

^cLaboratory for Chemical and Biological Crystallography, Ruđer Bošković Institute, 10 000 Zagreb, Croatia



ARTICLE INFO

Article history:

Received 22 December 2020

Revised 4 March 2021

Accepted 15 March 2021

Available online 23 March 2021

Keywords:

ruthenium
chalcone
pyridine
organometallic
X-ray diffraction
infrared
DNA
BSA

ABSTRACT

The chiral-at-metal, piano-stool ruthenium(II) racemic organometallic [Ru(cymene)(chalconato)(pyridine)]PF₆ was prepared by a multistep solution synthesis and its molecular and crystal structure was determined by single crystal X-ray diffraction. The compound crystallizes in a centrosymmetric triclinic *P*-1 space group with two molecules of opposite chirality within the asymmetric unit. Ruthenium is embedded in an octahedral half-sandwich coordination environment with four different donors, which generates the chirality of the metal centre. The formation of the organometallic was monitored *ex-situ* by infrared spectroscopy. The pyridine coordination to Ru(II) was particularly analysed to find its characteristic marker bands. The complex was also characterized by elemental analysis and NMR spectroscopy in solution. Its interaction with CT DNA and bovine serum albumin (BSA) was investigated by electron spectroscopy and spectrofluorimetry. The organometallic binds to DNA predominantly by electrostatic forces with low *K_b* value. On the contrary, its high affinity for BSA was confirmed by strong fluorescence quenching. The synchronous emission spectra revealed that the microenvironment of tryptophan is more affected compared to the environment of tyrosine.

© 2021 Elsevier B.V. All rights reserved.

1. Introduction

The focus of inorganic chemistry in the 21st century is synthesis – structure – (re)activity correlation as a prerequisite for understanding chemical dynamics at the molecular level and reaching the point from where desired properties of the new compounds can be controlled. Arising from this concept, ruthenium(II) organometallic compounds were extensively studied as potential candidates for the design and development of highly efficient catalysts [1] and drugs [2–4]. The properties of pseudo octahedral piano-stool organometallics with general formula [(arene)Ru^{II}XYZ] are controlled through arene/ligand replacement and modification of the aliphatic or aromatic ligand denticity, as well as by donor atoms type that occupy three coordination positions designated as X, Y and Z [5–7]. Due to the steric limitations of many tridentate ligands, X, Y and Z positions usually belong to one bidentate and one monodentate ligand, resulting in a vast structural diversity of these compounds. Moreover, if the donor atoms at the X, Y and

Z positions are all different, the chirality is generated at the central ruthenium atom which opens additional avenues of application of such chemical edifices as catalysts of enantioselective organic transformations [8].

Because of their structure, chalcones are prominent building blocks for cancer [9], malaria [10], tuberculosis [11] and cardiovascular diseases [12] drug design. The corresponding ruthenium-chalcone compounds, on the other hand, exhibited catalytic activity in hydrogenation of ketones and oxidation of alcohols [13], as well as in reactivity toward DNA, nuclease activity [14], cytotoxicity [15,16] and antileukemia activity [17] which, combined, greatly encouraged further investigation of these compounds. The coordination of heterocycles to ruthenium proved to be crucial in designing the compounds with antitumor activity for which NAMI-A and KP1019 are probably the best examples [18,19]. Heterocycles are highly convenient, usually monodentate ligands that allow fine-tuning of kinetic, electronic, steric or redox properties of coordination compounds. However, monitoring of heterocycle coordination to a metal centre in a multistep synthesis can be demanding and requires time-consuming techniques such as NMR. Fast and widely available infrared spectroscopy is rarely used to monitor heterocy-

* Corresponding author at: Laboratory for Chemical and Biological Crystallography, Ruđer Bošković Institute, Bijenička cesta 54, HR-10000 Zagreb.

E-mail address: aleksandar.visnjevac@irb.hr (A. Višnjevac).

cle coordination since the marker bands are usually of lower intensity and overlapped by bands of other ligands.

Many ruthenium complexes are extensively investigated as very promising antitumor agents. The most representative examples include chlororuthenium(III) coordination complexes featuring heterocycles as coligands, such as KP1019 and NAMI-A, and the organometallic compound of ruthenium(II) with triazaphosphadamantane known as RAPTA. These compounds are known to bind to DNA and proteins which are believed to be their biological targets *in vivo* [20–22], and the investigation of their interaction with new compounds is usually the first step of the biological evaluation. Anticancer activity of ruthenium-arene compounds *in vitro* can be improved in the presence of proteins. A good example is the case of RM175 ($[(\eta^6\text{-biph})\text{RuCl}(\text{en})]^+$) whose cytotoxicity towards highly-invasive breast MDA-MB-231, human breast MCF-7 and human epithelial HBL-100 cancer cells is enhanced in the presence of human serum albumin [23]. Also, ligand substitutions between ruthenium-cymene compounds can control protein *versus* DNA targeting and consequently anticancer activity. This is best illustrated for two ruthenium-cymene compounds: RAED-C and RAPTA-C. RAED-C ($[(\text{cym})\text{RuCl}(\text{en})]^+$) is cytotoxic toward primary tumours and targets DNA of chromatin, while RAPTA-C ($[(\text{cym})\text{RuCl}_2(\text{PTA})]$) is relatively non-cytotoxic antimetastatic compound which preferentially forms adducts on the histone proteins [24]. The protein *versus* DNA binding was also investigated for many other ruthenium organometallics such as those of NS donor Schiff bases [25], anthracenyl-appended diazacycloalkanes [26], substituted pyridylimidazo[1,5-a]pyridines [27], ethylenediamine [28], chloroquine [29], and diimines [30].

Here we report on the synthesis, chemical characterization and crystal structure of the racemic chiral-at-metal organometallic compound of ruthenium(II) having 2'-hydroxychalcone ligand and pyridine as coligand, as well as *ex-situ* infrared monitoring of its formation. The interaction of newly prepared ruthenium organometallic with CT DNA and with bovine serum albumin (BSA) was investigated.

2. Experimental

2.1. Chemicals

All chemicals used in this study were obtained from commercial sources at highest degree of purity available and used as received. Dichloro(*p*-cymene)ruthenium(II) dimer was prepared according to published procedure [31]. 2'-hydroxychalcone was obtained as a condensation product of benzaldehyde and 2'-hydroxyacetophenone from Claisen-Schmidt condensation [32]. Deuterated chloroform ($\text{CDCl}_3\text{-}d$ with *v/v* 0.03% TMS, 99.80% D) for NMR spectroscopy was purchased from Euriso-Top, France. Highly polymerized deoxyribonucleic acid sodium salt from calf thymus (CT DNA), Type I, fibers ($A_{260}/A_{280} > 1.8$) was obtained from Sigma. Bovine serum albumin (BSA, $\geq 98\%$) was obtained from Sigma as a lyophilized powder.

2.2. Physical measurements

Infrared spectra were collected in transmission mode by the KBr pellet technique using Perkin Elmer BX FTIR. The course of the reaction was monitored by withdrawing the microliter aliquots of the reaction mixture and evaporating the solvent after which KBr pellets were prepared. CHN analyses were performed on a Perkin-Elmer 2400 Series II CHNS analyser.

The NMR spectra of the chalcone ligand (**e**) were recorded on Bruker AV600 spectrometer, and NMR spectra of the organometallic (**f**) were recorded on Bruker AV300 spectrometer, both with a 5 mm observed RT probe in $\text{CDCl}_3\text{-}d$. Used spectrometers operate

at 600.130 MHz and 300.133 MHz for the ^1H , and 150.903 MHz and 75.475 MHz for the ^{13}C nucleus. Chemical shifts, in ppm, are referred to tetramethylsilane (TMS) as internal standard. Assignment of ^1H and ^{13}C NMR signals was performed using two-dimensional homo- and heteronuclear correlation experiments with standard parameters: ^1H - ^1H Correlation Spectroscopy (COSY), ^1H - ^1H Nuclear Overhauser Effect Spectroscopy (NOESY), ^1H - ^{13}C Heteronuclear Multiple Quantum Coherence (HMQC) and ^1H - ^{13}C Heteronuclear Multiple Bond Correlation (HMBC).

Single crystal X-ray data collection was conducted at RT, on an Oxford diffraction Xcalibur Nova Ruby device. Cu radiation ($\lambda = 1.54184 \text{ \AA}$) was employed. Data reduction and cell refinement were carried out using CRYSTALIS PRO software [33]. Structure was solved by direct methods with SIR2014 [34] and refined by a full matrix least-squares refinement based on F^2 , with SHELXL [35]. Molecular illustrations were prepared with MERCURY [36]. Calculations of molecular geometries and crystal packing parameters were performed with PLATON [37]. All software used is included into the WinGX package [38]. Hydrogen atoms were included in their geometrically calculated positions and refined according to the riding model, or (where sustainable throughout the refinement) located from the difference map and refined freely. Multi-scan absorption correction procedure was applied [39]. Powder X-ray diffraction data was collected at RT on Bruker D8 Discover diffractometer equipped with LYNXEYE XE-T detector, in Bragg-Brentano geometry. Data were collected in 2θ range $5 - 50^\circ$. Rietveld structure refinement was performed in HighScore Xpert Plus program 3.0. Refinement was carried out by using the split-type pseudo-Voigt profile function and the polynomial background model. Isotropic vibration modes were assumed for all atoms. During the refinement, a zero shift, scale factor, half-width parameters, asymmetry and peak shape parameters were simultaneously refined.

Interaction of organometallic (**f**) with DNA and BSA was observed in 10 mM Tris-HCl buffer at pH 7.42 and at RT. Stock solution of organometallic (**f**) was prepared in methanol at concentration 2 mM. The spectroscopic titration of compound with CT DNA was carried out by adding 10 μL aliquots of DNA (6.67 mM) to organometallic solution (2.000 mL, 5×10^{-5} M). Each spectrum was recorded after 2-minutes equilibration time. The titration of CT DNA with organometallic (**f**) was performed by adding 5 μL aliquots of organometallic (2 mM) to the solution of CT DNA (2.000 mL, 1.67×10^{-4} M). The incubation of organometallic (**f**) with CT DNA (1.67×10^{-4} M) was carried out at 2:1 [DNA]/[organometallic] ratio.

Spectrofluorimetric titration of BSA with organometallic (**f**) was carried out by adding 10 μL aliquots of organometallic (0.2 mM) to solution of BSA (2.000 mL, 3.68×10^{-6} M) and recording emission spectra in 290 – 430 nm range with 279 nm as excitation wavelength. The synchronous spectra were recorded under the similar conditions as described above while recording the emission spectra in range 250 – 310 nm with $\Delta\lambda = 15$ nm and $\Delta\lambda = 60$ nm.

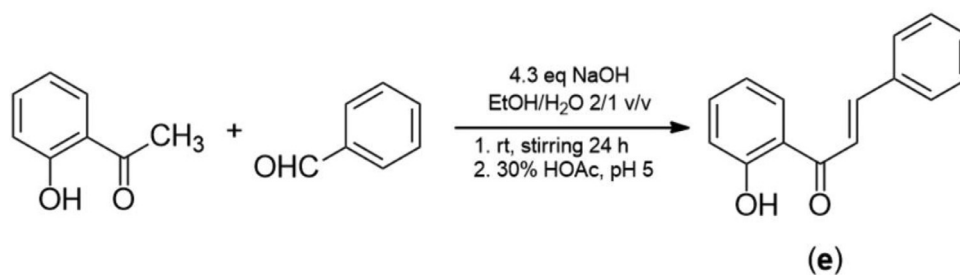
2.3. Synthesis

Synthesis of chalcone (**e**)

2'-hydroxyacetophenone (20 mmol, 2.723 g) and benzaldehyde (20 mmol, 2.123 g) were dissolved in ethanol (40 mL), aqueous solution of sodium hydroxide (86 mmol, 5 M, 17.2 mL) was added portion-wise and the mixture was vigorously stirred for 24 hours. The orange solution was acidified to pH 5 using acetic acid. The resulting yellow chalcone was filtered off, washed with water, and recrystallized from hot ethanol. Yield: 3.53 g (79%).

Synthesis of organometallic $[(\text{cym})\text{Ru}(\text{chalc})(\text{py})]\text{PF}_6$ (**f**)

Pyridine (48 μL , 0.60 mmol) was added to a vigorously stirred cold suspension of $[\text{RuCl}_2(\text{cym})]_2$ (184 mg, 0.30 mmol) in acetone (10 mL) causing an immediate precipitation of or-



Scheme 1. Synthesis of 2'-hydroxychalcone (e).

ange [(cym)RuCl₂(py)]. Stirring was continued for a half hour after which silver triflate (308 mg, 1.20 mmol) dissolved in acetone (10 mL) was added portion-wise to the reaction mixture. Approximately a quantitative amount of silver chloride (170 mg) was filtered off through a blue ribbon and the resulting orange filtrate was mixed with dichloromethane solution (10 mL) of previously deprotonated chalcone ligand (135 mg, 0.60 mmol) with triethylamine (84 μ L, 0.60 mmol). The obtained intensively red solution was stirred at room temperature for 24 hours and evaporated to dryness under reduced pressure. The oily product was dissolved in chloroform (15 mL), transferred to a separating funnel, and washed with water (2 \times 15 mL). The chloroform layer was dried over anhydrous sodium sulphate, filtered and evaporated to dryness under reduced pressure. The residue was dissolved in methanol (5 mL), and methanol solution (3 mL) of sodium hexafluorophosphate (500 mg) was added. The resulting red substance was filtered off, washed with a water-methanol mixture (1/1, v/v, 2 \times 2 mL) and dried under vacuum over silica. The mother liquor gave single crystals of (f) as dark red prisms upon an overnight slow evaporation at room temperature. Yield: 285 mg (69%). *Anal. cal.* for C₃₀H₃₀F₆NO₂PRu (682.59): C 52.79; H 4.43; N 2.05. Found: C 52.74; H 4.33; N 2.16%. ¹H NMR (300 MHz, CDCl₃, 25°C): δ 8.63 (2H, dd, *J* = 6.29, 1.26 Hz, H-26 and H-30), 8.18 (1H, d, *J* = 15.37 Hz, H-7), 7.80 (2H, dd, *J* = 7.30, 2.50 Hz, H-2 and H-6), 7.72 (1H, dd, *J* = 7.54, 1.39, H-28), 7.45–7.37 (7H, m, H-3 and H-5, H-4, H-8, H-11, H-27 and H-29), 7.25 (1H, ddd, *J* = 8.52, 6.71, 1.54 Hz, H-13), 6.98 (1H, d, *J* = 8.66 Hz, H-14), 6.45 (1H, ddd, *J* = 7.96, 6.57, 0.97 Hz, H-12), 5.89 (1H, d, *J* = 6.09 Hz, H-17 or H-19), 5.65 (1H, d, *J* = 6.09 Hz, H-17 or H-19), 5.58 (1H, d, *J* = 6.09 Hz, H-16 or H-20), 5.54 (1H, d, *J* = 6.09 Hz, H-16 or H-20), 2.79 (1H, septet, *J* = 6.88 Hz, H-23), 2.07 (3H, s, H-22), 1.34 (3H, d, *J* = 6.88 Hz, H-24 or H-25), 1.25 (3H, d, *J* = 6.88 Hz, H-24 or H-25) ppm; ¹³C NMR (75 MHz, CDCl₃, 25°C): δ 187.2 (1C, C-9), 170.4 (1C, C-15), 152.6 (2C, C-26 and C-30), 147.8 (1C, C-7), 139.0 (1C, C-28), 137.2 (1C, C-13), 134.9 (1C, C-1), 131.5 (1C, C-4), 131.3 (1C, C-11), 129.3 (4C, C-2 and C-6, C-3 and C-5), 126.2 (2C, C-27 and C-29), 124.7 (1C, C-14), 121.0 (1C, C-8), 120.4 (1C, C-10), 116.0 (1C, C-12), 102.1 (1C, C-18), 99.6 (1C, C-21), 85.3 (1C, C-17 or C-19), 84.4 (1C, C-17 or C-19), 81.9 (1C, C-16 or C-20), 81.0 (1C, C-16 or C-20), 31.0 (1C, C-23), 22.5 (2C, C-24 and C-25), 17.8 (1C, C-22) ppm.

In order to check the phase purity, crystalline material, as obtained from the mother liquid, was examined by the X-ray powder diffraction. Fig. S1 shows Rietveld refinement using the structural model as determined from single crystal analysis; no additional reflections can be noted thus confirming the bulk sample contain [(cym)Ru(chalc)(py)]PF₆ exclusively.

3. Results and discussion

3.1. Synthesis

The base-catalysed condensation of 2'-hydroxyacetophenone and benzaldehyde in aqueous ethanol gave yellow 2'-hydroxychalcone as shown in Scheme 1.

Table 1
Crystallographic data

Structure	[(cym)Ru(chalc)(py)]PF ₆ (f)
Brutto formula	C ₃₀ H ₃₀ F ₆ NO ₂ PRu
Form. weight (g mol ⁻¹)	682.59
Crystal colour, habit	dark red, prism
Crystal dim. (mm)	0.20 \times 0.25 \times 0.35
Crystal density (g cm ⁻³)	1.53
Space group	P-1
<i>a</i> (Å)	12.7053 (3)
<i>b</i> (Å)	15.0340 (4)
<i>c</i> (Å)	15.7685 (3)
α (°)	94.879 (2)
β (°)	90.910 (2)
γ (°)	97.963 (2)
<i>V</i> (Å ³)	2970.95 (12)
<i>Z</i>	4 (<i>Z'</i> =2)
<i>R</i> _{int}	0.0428
<i>R</i> _{σ}	0.0640
μ (CuK α) (mm ⁻¹)	5.37
<i>F</i> (000)	1384
θ max (°) data col.	75.91
<i>hkl</i> limits of data col.	-15,15;-18,18;-19,13
No. refl. Unique	12240
No. refl. obs. [<i>I</i> >2 σ (<i>I</i>)]	10762
Parameters	777
<i>R</i> ₁ , all	0.0463
<i>R</i> ₁ [<i>I</i> >2 σ (<i>I</i>)]	0.0415
<i>wR</i> ₂ , all	0.1116
<i>wR</i> ₂ [<i>I</i> >2 σ (<i>I</i>)]	0.1055
<i>S</i>	1.103
ρ _{max} , ρ _{min} (e Å ⁻³)	0.75; -1.10

The organometallic, chiral-at-metal [(cym)Ru(chalc)(py)]PF₆ (f) was prepared by a multistep solution synthesis and isolated as racemic mixture (Scheme 2). Complete synthetic procedure was carried out at normal environmental conditions without the usage of an inert gas atmosphere. In the first step, the parent ruthenium dimer [RuCl₂(cym)]₂ (a) was reacted with one equivalent of pyridine (b) in acetone affording the neutral [RuCl₂(cym)(py)] (c). Then the chlorides were precipitated by the addition of two equivalents of silver triflate. The chalcone ligand (e) was deprotonated with triethylamine and reacted with *in situ* prepared ruthenium-acetone intermediate (d). The mono cationic [(cym)Ru(chalc)(py)]⁺ (f) was separated from Et₃NHCF₃SO₃ by chloroform-water extraction and precipitated from the organic solvent by the addition of aqueous sodium hexafluorophosphate. The reaction steps are shown in Scheme 2.

3.2. Molecular and crystal structure

Experimental data collection details, as well as crystallographic parameters are given in Table 1, selected torsional angles illustrating conformational differences between two molecules of the asymmetric unit are given in Table S1, while the hydrogen bonds are listed in Table S2. Fig. 1 depicts molecular structure of (f). The

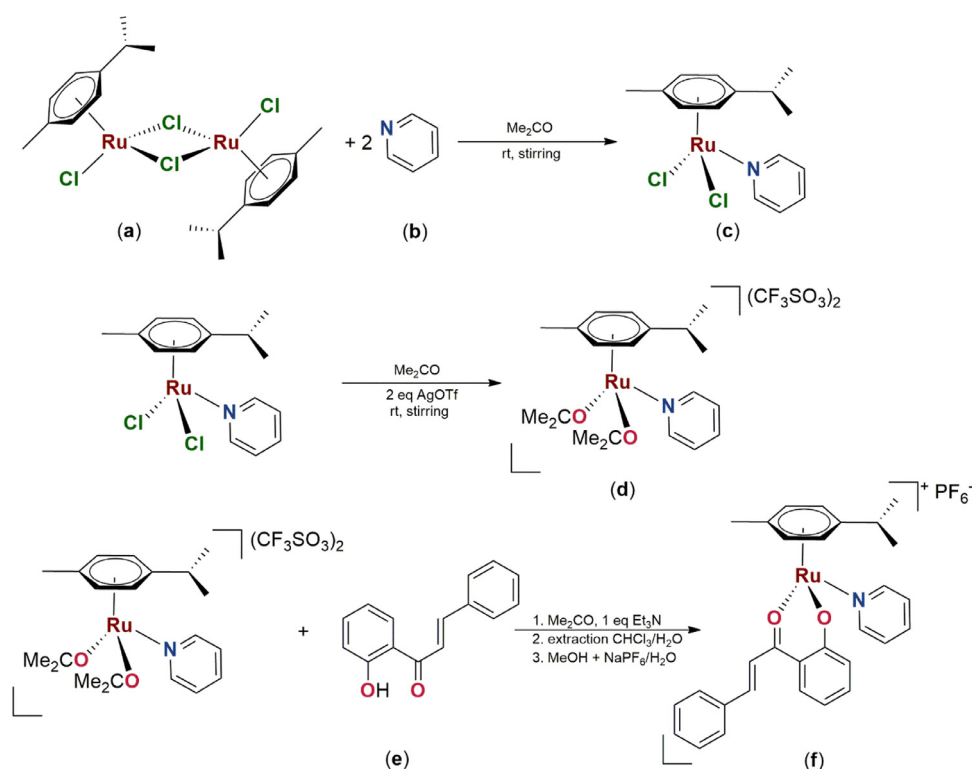
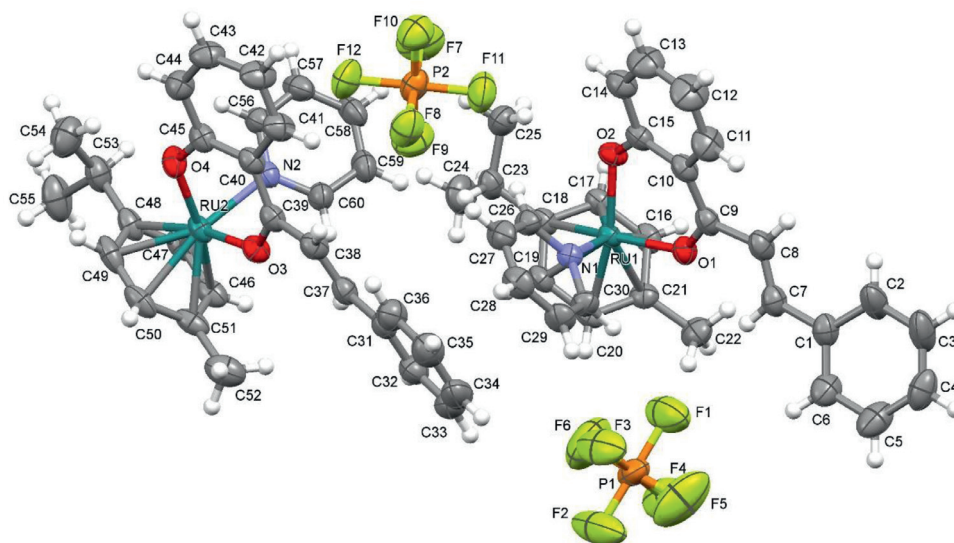
Scheme 2. Synthesis of [(cym)Ru(chalc)(py)]PF₆.

Fig. 1. ORTEP drawing of (f) with atom numbering. Thermal ellipsoids are scaled at 40% probability level for clarity.

overlay of the two molecules of the asymmetric unit is given in Fig. 2.

Compound (f) crystallizes in centrosymmetric triclinic *P*-1 space group with two molecules of opposite chirality per asymmetric unit. Pseudo-octahedrally coordinated ruthenium, which sits in a centre of a piano-stool coordination environment with four different donors is a chiral centre in this molecule and generates the overall molecular chirality of the complex. While one face of the pseudo-octahedron around Ru(II) is occupied by the donor *p*-cymene phenyl ring, the remaining face comprises three coordinated donor atoms: pyridine nitrogen and two oxygen atoms from the chalcone moiety: carbonyl oxygen and deprotonated hydroxyl

oxygen. The complexes featuring this type of coordination environment are also known in literature as half-sandwich complexes [40]. Free rotation around the C1–C7 *i.e.* around C31–C37 bonds enables different orientations of the chalcone phenyl moiety with respect to the remaining of the complex molecule which may explain the unusually high *Z* number (4). Indeed, values of the corresponding analogous torsion angles differ significantly for two molecules of the asymmetric unit (Table S1). One of the PF₆[−] anions (P1) reveals large thermal ellipsoids of the fluorine atoms, which suggests multiple orientations (at least two), which, however, are not crystallographically distinct. Structure of (f) does not feature classic hydrogen bonds. Nevertheless, a number of intramolecular and

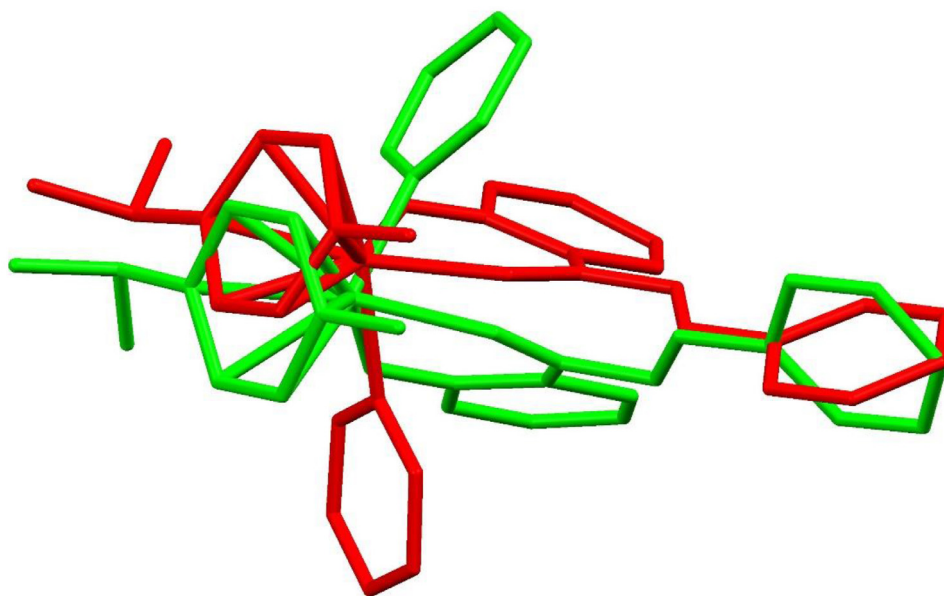


Fig. 2. Overlay of two molecules within the asymmetric unit of (f) reveals their opposite chirality and conformational flexibility.

intermolecular C–H \cdots O and C–H \cdots F interaction are responsible for a highly complex 3D molecular network characterizing this crystal structure (Table S2).

3.3. Infrared spectra

All reactions in applied multistep synthesis (Scheme 2) were monitored by IR spectroscopy. Particular challenge was to observe the coordination of pyridine to Ru(II) ion because of extensive overlapping and lower bands intensity of nonpolar heterocycles in the IR spectra [41–44]. Recorded infrared spectra of parent compounds (a)–(e), complex (f) and NaPF₆ are shown in Fig. S2 with the selected infrared data summarized in Table S4.

Several weak intensity bands just below 3000 cm⁻¹ arise from C–H stretching vibrations of cymene saturated methyl and isopropyl groups. This is the only region in IR spectra with no overlap with bands of other ligands and thus can be used to confirm the presence of cymene moiety. The presence of other ligands in the first coordination sphere of ruthenium does not significantly affect the position of these bands. The evidence of chalcone coordination to Ru(II) is shifting ν (C=O) and ν (C–O(H)) bands upon coordination. Strong absorption band located in the ligand spectrum at 1640 cm⁻¹ is shifted for 16 cm⁻¹ toward lower wavenumbers upon coordination and is found in the spectrum of complex (f) at 1624 cm⁻¹. This is a direct result of the C=O bond weakening as a result of chalcone coordination to Ru(II) through carbonyl oxygen. On the other hand, the band arising from ν (C–O(H)) stretching, found at 1339 cm⁻¹ in the spectrum of ligand (e), is shifted to higher wavenumbers upon coordination, as a result of the strengthening of C–O bond due to the deprotonation of phenolic O–H group and formation of weaker Ru–O bond.

The bands found in the spectrum (f) at 425 and 661 cm⁻¹ (Fig. S3), according to Nakamoto's literature data were attributed to ring rocking mode and out of plane pyridine vibrations, respectively [45]. Both bands are weak and found in the low frequency region, where many otherwise symmetry-forbidden vibrations, are awakened upon ligand coordination, due to the reduced symmetry. Two other bands located at 748 and 700 cm⁻¹ in the spectrum of pyridine, with moderate and strong intensity, respectively, arise from C–H out of plane vibrations and are particularly useful for estimation of the pyridine presence in isolated coordination

species. However, they are unaffected by coordination and based solely on them it is impossible to conclude whether the pyridine is present as a coordinated ligand, impurity or solvate. Another relatively insensitive band in connection with the coordination of pyridine to metal was found in the region relatively free of vibrations of other ligands is a band assigned to C–H stretching vibrations at 3080 cm⁻¹. This band is somewhat higher positioned with respect to those arising from other aromatic C–H vibrations (usually found between 3000 and 3050 cm⁻¹). However, its low intensity makes it relatively insecure for pyridine presence claim. The band that was found to be the most indicative marker for pyridine coordination to metal centre is a mid-region strong intensity band at 1439 cm⁻¹ arising from pyridine ring deformation (in-plane C–H wagging). This band does not overlap with bands arising from cymene or chalcone moieties and has a medium intensity in the spectrum of a coordination compound. Moreover, it is shifted to higher wavenumbers upon coordination thus undoubtedly confirming the presence of coordinated pyridine. The infrared bands originating from hexafluorophosphate vibrations are easy to identify since they are generally of strong intensity. The band at 840 cm⁻¹ arises from P–F bond stretching, while the band at 558 cm⁻¹ is attributed to F₂P deformation.

3.4. NMR spectroscopy

In the recorded ¹H and ¹³C NMR spectra of compounds (e) and (f) only one set of signals was observed (Figs. 3 and S4–S7). Complexation of hydroxychalcone (e) to ruthenium(II) ion was confirmed by difference in the ¹H and ¹³C atom signal chemical shifts between ligand (e) and complex (f), and by lack of the OH group signal in the complex (f) proton spectrum.

The biggest changes in ¹³C chemical shifts were observed for the C-15 ($\Delta\delta_{\text{coord}} = -6.7$ ppm) and C-9 ($\Delta\delta_{\text{coord}} = 6.6$ ppm) atom signals indicating O,O-chelating binding of the chalcone moiety to the ruthenium(II) ion. The difference in atom signals chemical shifts after complexation was also noticed for *para*-cymene: aromatic ring H-atoms and H-25 were unshielded ($\Delta\delta_{\text{coord}} = 0.41$; 0.06 ppm) and H-21 and H-27 were shielded ($\Delta\delta_{\text{coord}} \approx -0.09$;

-0.03 ppm). Pyridine molecule binds to the Ru(II) ion through the nitrogen lone electron pair, and the rest of the ¹H ring atom signals were unshielded ($\Delta\delta_{\text{coord}} < 0.06$ ppm). Observed in-

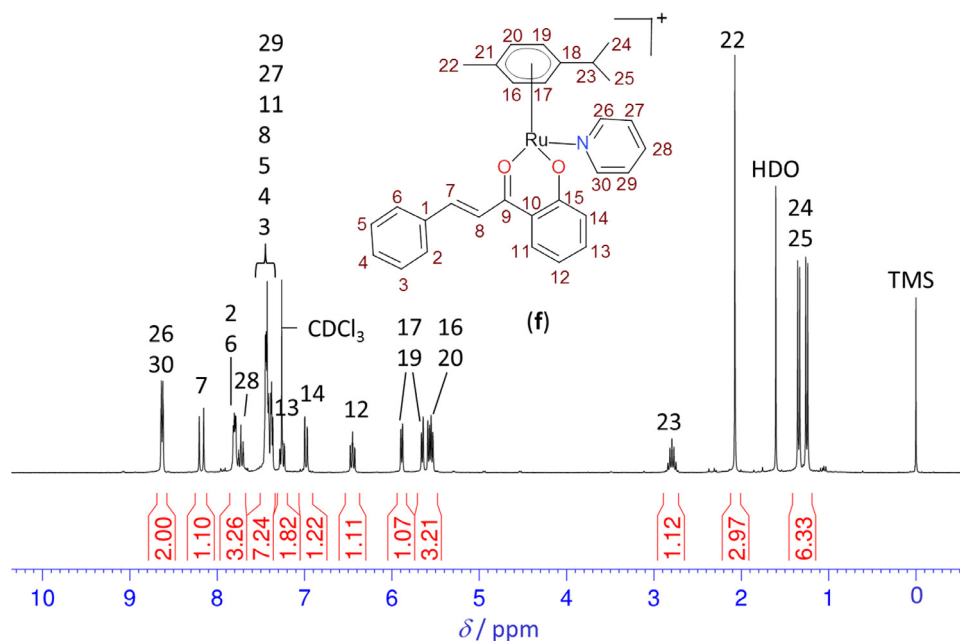
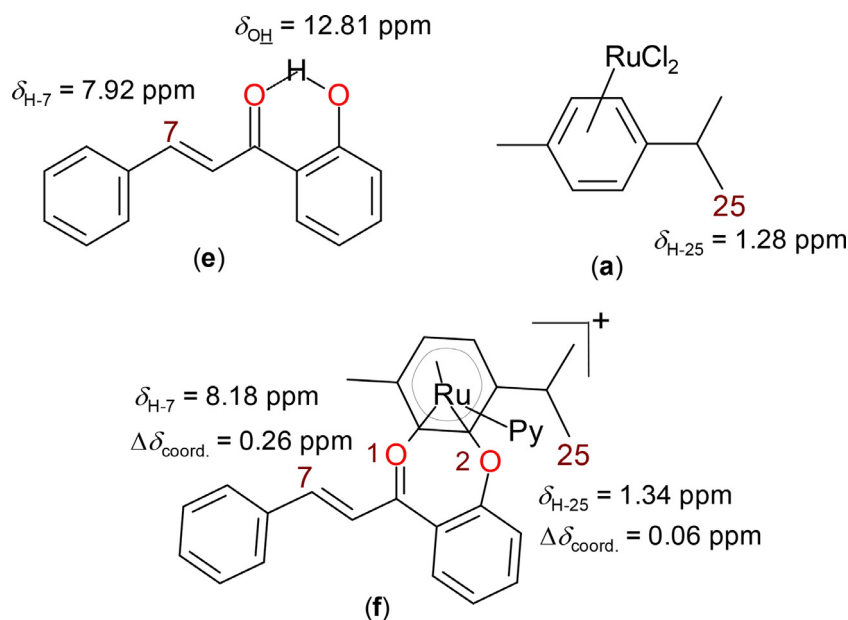


Fig. 3. 300 MHz ^1H NMR spectrum with assignments and numeration scheme of (f).



Scheme 3. H-7 and H-25 atom signals chemical shift changes ($\Delta\delta_{\text{coord.}}$) in the ^1H NMR spectrum before ((a), (e)) and after complexation (f); $\Delta\delta_{\text{coord.}} = \delta_{\text{complex}} - \delta_{\text{ligand}}$.

tramolecular NOE cross peaks between pyridines H-26 and H-30 atoms and H-22, H-23, H-24, H-25 of *para*-cymene, and H-14 of chalcone moiety confirmed also the half-sandwich conformation of (f) in the solution. Coordination effect was observed for H-7 and H-25 atom signals which were unshielded for 0.26 ppm and 0.06 ppm, respectively. It is in accordance with hydrogen interaction found by X-ray, and in the solution NMR it was attributed to the steric effect of oxygen atoms, O-1 and O-2, which are probably getting closer to H-7 (O-1) and H-25 (O-2) after breaking ligand strong hydrogen bond O-1 \cdots H-O-2 ($\delta = 12.81$ ppm) when binding to metal ion (Scheme 3). All other chalcone atom signals in ^1H NMR spectra were shielded ($\Delta\delta_{\text{coord.}} = -0.20$ – -0.50 ppm). Despite a large signal overlap (7H) in the range 7.45–7.37 ppm, all complex peaks were assigned by means of the 2D NMR methods (COSY, NOESY, HMQC, HMBC); Figs. S8–S11.

3.5. Electronic spectra

The electronic spectra of ligands (chalcone and pyridine), parent ruthenium compound and ruthenium organometallic (f) are shown in Fig. S3. The electronic spectrum of (f) is dominated by two strong absorption bands, one medium intensity band and one shoulder in 200 – 600 nm region. The medium intensity band is located in visible spectrum with maximum near 490 nm and arises from MLCT transitions [$\text{Ru}(4d\pi) \rightarrow \pi^*(\text{ligand})$]. The band at 316 nm in the spectrum of chalcone ligand can be assigned to $n \rightarrow \pi^*$ transitions. Upon coordination of chalcone to ruthenium this band is shifted to higher wavelength and is found at 322 nm in the spectrum of (f). The bathochromic (red) shift of 6 nm is a consequence of deprotonation of the chalcone phenolic group and coordination to Ru(II) [14,46]. Very wide shoulder in spectrum of (f) (220 – 270

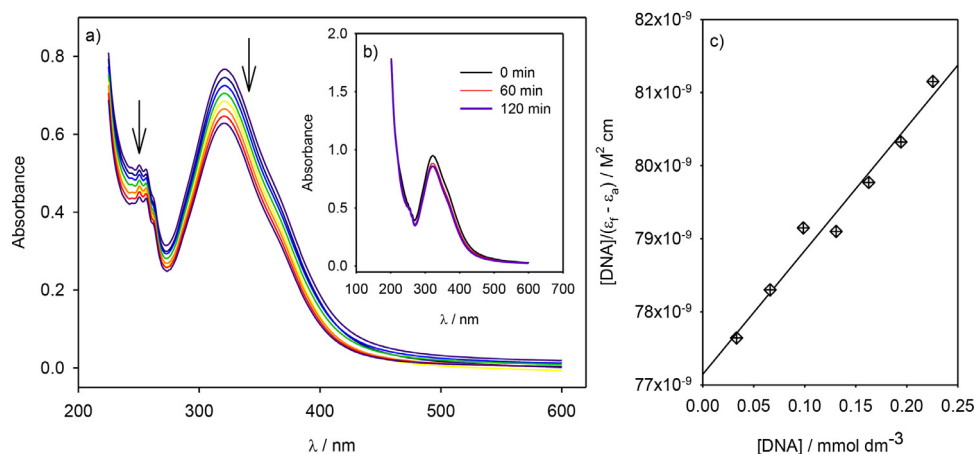


Fig. 4. Interaction of organometallic (**f**) with CT DNA: a) spectroscopic titration of (**f**) with CT DNA; b) behaviour of (**f**) in buffered aqueous solution; c) graphical determination of binding constant of (**f**) with CT DNA.

nm) is the consequence of the superimposed absorptions corresponding to the transitions arising from pyridine (260 nm) and chalcone ligand (220 nm) [47]. The absorption band at 203 nm arises from $\pi \rightarrow \pi^*$ transitions of aromatic cores of all three aromatic ligands [48].

3.6. Interaction with DNA

The spectroscopic titration of (**f**) with increasing concentrations of CT DNA is shown in Fig. 4a. The moderate hypochromism without significant shift of the absorption maximum was observed at the band positioned near 320 nm. Fig. 4b demonstrates behaviour of (**f**) in aqueous solutions over time and indicates that the compound is hydrolytically inert. Thus, all changes in the electronic spectra of the compound (**f**) during the spectroscopic titration (Fig. 4a) can be addressed to interaction of (**f**) with CT DNA. The interaction of chalcone ligand (**e**) with CT DNA also showed moderate hypochromism without observable band shifting (Fig. S12).

The data corresponding to the titration experiment are summarized in Table S5 and the binding constant (K_b) of (**f**) with CT DNA was determined graphically from the plot $[DNA]$ vs $[DNA]/(\epsilon_f - \epsilon_a)$ as the slope/intercept ratio (Fig. 4c). The binding constant of (**f**) with CT DNA was determined as $4.47 \times 10^2 \text{ M}^{-1}$ and is tenfold lower compared to the one measured for chalcone ligand (**e**) ($4.67 \times 10^3 \text{ M}^{-1}$). The low value of binding constant indicates that the cationic organometallic (**f**) predominantly interacts with CT DNA through electrostatic pairing with negatively charged phosphate groups. The values of binding constant for groove binding and intercalation are significantly higher, having values $10^4 - 10^6 \text{ M}^{-1}$. Several other cationic ruthenium organometallics showed electrostatic binding mode to DNA such as those having ofloxacin [49], ethylenediamine [50] or bis(3,5-dimethylpyrazolyl) derivatives of benzoic acid [51] as ligands. Also, some non-arene organometallics of ruthenium(II) such those of 2-phenylpyridine prefer electrostatic binding mode [52]. On the other hand, planar π -conjugated aromatic system of chalcone (**e**) is suitable for groove binding and intercalation as it was observed for some anthraquinone-chalcone hybrids [53] and methoxy substituted 2'-hydroxychalcones [54].

To confirm the electrostatic binding mode of organometallic (**f**) with CT DNA, the titration experiment was carried out (Fig. 5a). The intensity of the absorption near 260 nm in electronic spectrum of CT DNA is directly related to DNA helix. The extinction coefficient of the single stranded DNA is higher ($7100 \text{ M}^{-1} \text{ cm}^{-1}$) as compared to double stranded DNA ($6600 \text{ M}^{-1} \text{ cm}^{-1}$) and absorbance increase at 260 nm indicates denaturation of DNA and

separation of the chains. On the contrary, the decrease of the absorbance at 260 nm indicates shortening of DNA chains due to electrostatic interactions. The titration experiment (Fig. 5a) shows that no significant changes in the secondary structure of DNA are observed within $[DNA]/[\text{organometallic}]$ ratio 25 – 3. However, at $[DNA]/[\text{organometallic}] = 2$, significant decrease of the absorbance was observed over time (Fig. 5b). The hypochromic effect at DNA absorption maximum (near 260 nm) is in correlation with conformational change of DNA and indicates shrinkage of helix in length as a consequence of the electrostatic interaction of (**f**) with DNA. This result is in a good correlation with the low K_b value obtained from spectroscopic titration of organometallic with CT DNA (Fig. 4). The percentage of the absorbance decrease over time was plotted in Fig. 5c. The curve clearly shows that the absorbance decrease is the highest over the first 15 minutes of the reaction, indicating that the binding of organometallic (**f**) to DNA is relatively fast.

3.7. Interaction with BSA

The interaction of chalcone ligand (**e**) and organometallic (**f**) with BSA was investigated spectrofluorimetrically utilizing the spectroscopic titration method. When the excitation of BSA was carried out at 279 nm, two amino acid residues, tryptophan and tyrosine, show intrinsic fluorescence with the emission maximum near 340 nm. Actually, the emission is mostly a consequence of the fluorescence of two sterically hindered tryptophan residues, Trp-134 in the first domain and Trp-212 in the second domain of BSA. Since the intensity and the position of the emission maxima is directly related to secondary structure of BSA, the changes in the emission spectrum can be addressed to their interaction with small molecules.

When the aqueous solution of BSA is titrated with organometallic (**f**) or chalcone ligand (**e**), the intrinsic fluorescence is quenched (Fig. 6a and Fig. S14a). The complexes (**f**) does not show intrinsic fluorescence in aqueous solution under the same conditions (Fig. S13). The quenching constant (K_{SV}) can be determined from Stern-Volmer equation graphically as the slope of $[\text{complex}]$ vs I_0/I plot (Fig. 6b and Fig. S14b). The quenching constant of (**f**) was determined to equal $2.23 \times 10^5 \text{ M}^{-1}$ indicating that the organometallic strongly quenches BSA fluorescence causing significant changes in polarity and conformation of tryptophan. The quenching constant of chalcone (**e**) is slightly lower ($1.30 \times 10^5 \text{ M}^{-1}$). The rate of quenching (k_q) was found to be $2.23 \times 10^{13} \text{ M}^{-1} \text{ s}^{-1}$ for organometallic (**f**) and $1.30 \times 10^{13} \text{ M}^{-1} \text{ s}^{-1}$ for chalcone (**e**) confirming that the quenching occurs in both cases through static mecha-

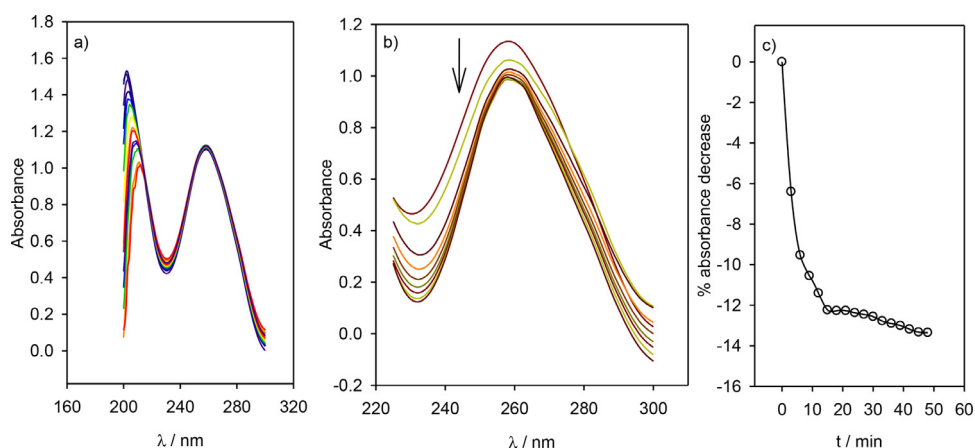


Fig. 5. Interaction of CT DNA with organometallic (**f**): a) spectroscopic titration of CT DNA with (**f**); b) electronic spectra of CT DNA over time during the incubation of CT DNA and (**f**) at 2:1 ratio; c) absorbance decrease at CT DNA absorption maximum over time during the incubation of CT DNA and (**f**).

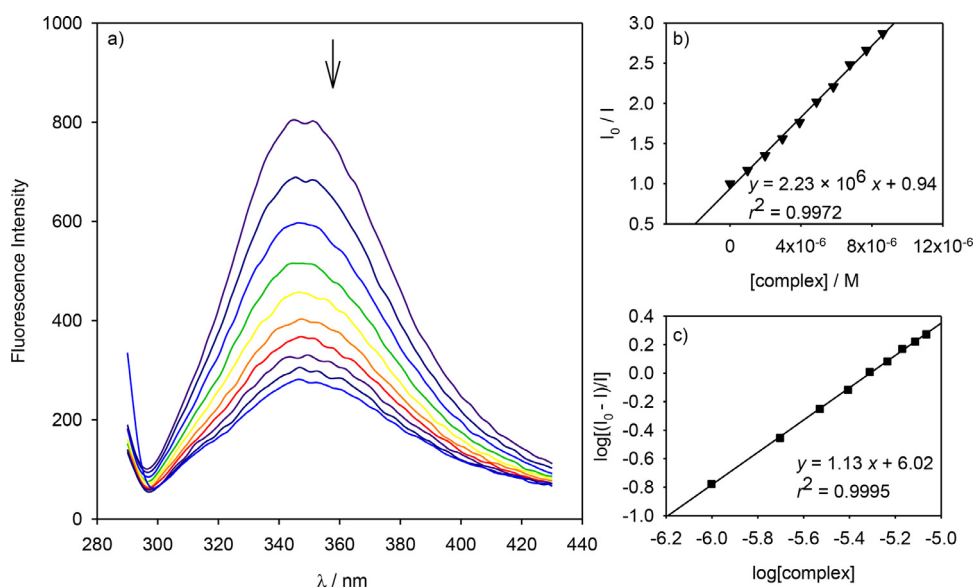


Fig. 6. Interaction of organometallic (**f**) with BSA: a) spectrofluorimetric titration of BSA with (**f**); b) graphical determination of Stern-Volmer constant; c) graphical determination of binding constant and number of binding sites.

nism, since the maximal value of k_q expected for dynamic quenching is $2 \times 10^7 \text{ M}^{-1} \text{ s}^{-1}$.

The number of binding sites (n) and the binding constant (K_b) were determined from $\log[\text{complex}]$ vs $\log[(I_0 - I)/I]$ plot (Fig. 6c and Fig. S14c). The number of binding sites was found to be close to 1, indicating that the organometallic (**f**) prefers binding with BSA in 1:1 ratio as many other small molecules. The binding constant of $1.04 \times 10^6 \text{ M}^{-1}$ demonstrates that organometallic (**f**) strongly binds BSA. The binding constant value is comparable to the values for drugs such as ibuprofen ($K_b = 3.6 \times 10^6 \text{ M}^{-1}$) and diazepam ($K_b = 1.6 \times 10^6 \text{ M}^{-1}$), which are known to bind albumin very tightly [55,56]. On the other hand, binding constant of chalcone (**e**) with BSA was determined as $1.88 \times 10^4 \text{ M}^{-1}$ and is fiftyfold lower compared to the one observed for organometallic (**f**). However the binding constant value is comparable to fluoro substituted chalcones ($(3.74 - 4.81) \times 10^4 \text{ M}^{-1}$) [57], but lower compared to non-substituted chalcone ($4.77 \times 10^5 \text{ M}^{-1}$) [58].

The binding constant of ruthenium(II) organometallic having chalcone and pyridine coligand to BSA is somewhat larger as compared to many other ruthenium-arene organometallics. The cyclopentadienylruthenium(II) compounds of acetophenone-4(*N*)-substituted thiosemicarbazone binding BSA with binding constant

in $1.03 \times 10^4 - 7.77 \times 10^5 \text{ M}^{-1}$ [25]. Also, benzene and cymene organometallics of ruthenium(II) with methylhomopiperazine derived ligands bind moderately strong to BSA ($1.7 \times 10^4 - 4.48 \times 10^4 \text{ M}^{-1}$) [26], while half-sandwich Ru(II) arene chloride-complexes of quinolin substituted benzo[*d*]imidazole, benzo[*d*]oxazole and benzo[*d*]thiazole bind BSA more strongly with binding constant in $3.63 \times 10^5 - 6.52 \times 10^5 \text{ M}^{-1}$ range [59]. Non-arene ruthenium organometallics of hydrazine ligands [60], 2-acetyl-5-chlorothiophene thiosemicarbazone [61] and binuclear thiosemicarbazone ruthenium complexes with 5-nitrofuryl pharmacophore [62] bind to BSA with 10^4 to 10^5 M^{-1} binding constants. The binding constant of $[\text{Ru}(\text{HL})(\text{CH}_3\text{CN})(\text{CO})(\text{PPh}_3)_2]$ with HL= 4-oxo-4*H*-pyran-2,6-dicarboxylic acid ($K_b = 2.89 \times 10^6 \text{ M}^{-1}$) is comparable to the binding constant of ruthenium(II) organometallic having chalcone and pyridine coligands [63].

As it was mentioned above, the fluorescence of the BSA arises from tryptophan and tyrosine. The distinction between the emission of these two amino acid residues can be made by synchronous spectroscopy, when the difference between the emission and excitation wavelength is fixed ($\Delta\lambda = \lambda_{\text{em}} - \lambda_{\text{ex}}$). If the $\Delta\lambda$ is set to 15 nm, the emission corresponds to tyrosine residues, while

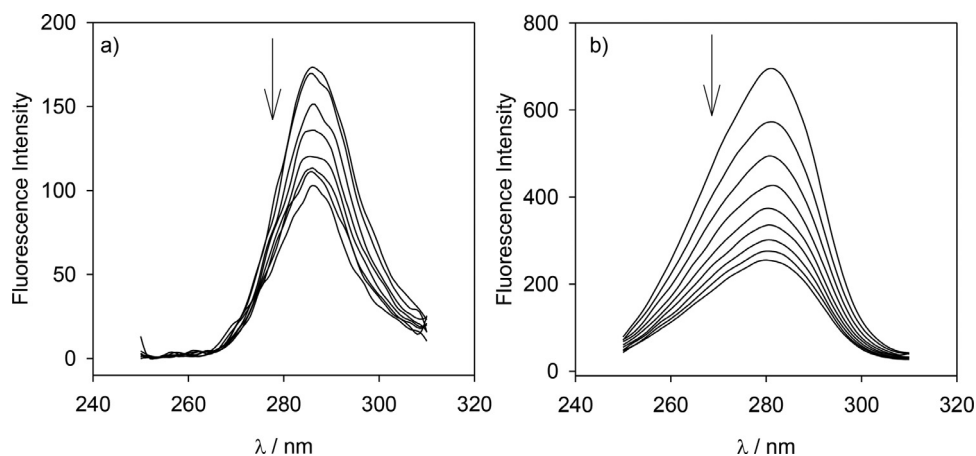


Fig. 7. Synchronous emission spectra of BSA in presence of increasing concentrations of (f) at: a) $\Delta\lambda = 15$ nm; b) $\Delta\lambda = 60$ nm.

the tryptophan emission is observed when $\Delta\lambda = 60$ nm [64]. The synchronous emission spectra of BSA in the presence of increasing concentrations of organometallic (f) and chalcone (e) are shown in Fig. 7 and Fig. S15, respectively. Both compounds induce emission decrease at both bands indicating that the microenvironment around tryptophan and tyrosine of BSA changes when the organometallic (f) or chalcone (e) are present. Under the same experimental conditions, the larger emission decrease at tryptophan emission maximum is observed in presence of complex (f) compared to ligand (e). Moreover, this decrease in presence of complex (f) is followed with small 1 nm hypochromic shift indicating that the binding of organometallic (f) to BSA disturbs tryptophan environment more than the one of tyrosine.

The higher affinity of (f) for BSA compared to DNA can be attributed to cationic, non-planar and hydrophobic nature of molecular ion of organometallic (f). The cationic nature dictates the electrostatic binding mode of (f) with DNA, while non-planar pseudo octahedral piano-stool conformation does not facilitate intercalation. The absence of heteroatoms, beyond those included in coordination to Ru, suitable for H-bond formation or other weak interactions of complex with DNA results in poor affinity of the complex to DNA and leaves electrostatic binding as the only possibility for interaction (f) with DNA. On the other hand, cationic nature of (f) facilitates binding with BSA but it is not decisive factor as in the case of DNA since BSA abounds with many surface available hydrophobic pockets [65,66] which accommodate hydrophobic interaction with lipophilic aromatic motives of organometallic (f).

4. Conclusions

The solution synthesis afforded cationic racemic chiral-at-metal organometallic ruthenium(II) compound fully characterized in the solid state and in the solution. The ruthenium(II) is embedded in pseudo-octahedral piano-stool conformation coordinated by cymene ligand in a η^6 -manner, bidentate monobasic chalcone ligand through phenolic and carbonyl oxygen atoms and the nitrogen atom of pyridine. The *ex-situ* monitoring of the pyridine coordination to Ru(II) by infrared spectroscopy revealed that band arising from pyridine ring deformation is the most useful marker for pyridine coordination. The interaction of organometallic with CT DNA revealed that synthesized compound only weakly binds to DNA by electrostatic interaction with negatively charged phosphate backbone and has lower affinity to DNA compared to parent chalcone ligand. The emission spectroscopy showed that the intrinsic fluorescence of BSA is strongly quenched in the presence of ruthenium organometallic and chalcone ligand. The high value of [(cym)Ru(py)(chalc)]PF₆ binding constant with BSA is

comparable to the one of commercial drugs such as ibuprofen and diazepam, and is fiftyfold higher as compared to parent chalcone ligand. The synchronous spectroscopy confirmed that the microenvironment around tryptophan is more affected as compared to the one of tyrosine. The results encourage further testing of [(cym)Ru(py)(chalc)]PF₆ for potential anticancer activity, especially due to the fact that it shows strong protein and low DNA binding affinity, which can be used in design of novel non-cytotoxic antimetastatic ruthenium organometallics. The higher affinity of our organometallic to BSA as compared to DNA can be associated with more hydrophobic nature of BSA compared to DNA.

Author statement

Aleksandar Višnjevac: X-ray structure determination, conceptualization, manuscript preparation

Sunčica Roca: NMR measurements and interpretation

Adnan Zahirović: Syntheses of the compounds, physicochemical measurements and interpretation (with the exception of NMR and single crystal X-ray studies), interaction with BSA and DNA assays

Emira Kahrović: conceptualization, manuscript preparation

Supplement

CCDC 2041048 contain the supplementary crystallographic data. These data can be obtained free of charge via <http://www.ccdc.cam.ac.uk/conts/retrieving.html>, or from the Cambridge Crystallographic Data Centre, 12 Union Road, Cambridge CB2 1EZ, UK; fax: (+44) 1223-336-033; or e-mail: deposit@ccdc.cam.ac.uk.

Declaration of Competing Interest

The authors declare that they have no known competing financial interests or personal relationships that could have appeared to influence the work reported in this paper.

Acknowledgements

The authors gratefully acknowledge the contribution of Dr. Jasminka Popović for the PXRD analysis.

Supplementary materials

Supplementary material associated with this article can be found, in the online version, at doi:10.1016/j.molstruc.2021.130326.

References

- [1] I. Arends, Ruthenium catalysts and fine chemistry, Springer Science & Business Media, 2004.
- [2] S. Thota, D.A. Rodrigues, D.C. Crans, E.J. Barreiro, Ru(II) compounds: next-generation anticancer metallotherapeutics? *Journal of Medicinal Chemistry* 61 (14) (2018) 5805–5821.
- [3] G. Gasser, N. Metzler-Nolte, The potential of organometallic complexes in medicinal chemistry, *Current Opinion in Chemical Biology* 16 (1–2) (2012) 84–91.
- [4] W.H. Ang, A. Casini, G. Sava, P.J. Dyson, Organometallic ruthenium-based antitumor compounds with novel modes of action, *Journal of Organometallic Chemistry* 696 (5) (2011) 989–998.
- [5] R. Fernández, M. Melchart, A. Habtemariam, S. Parsons, P.J. Sadler, Use of Chelating Ligands to Tune the Reactive Site of Half-Sandwich Ruthenium(II)-Arene Anticancer Complexes, *Chemistry—A European Journal* 10 (20) (2004) 5173–5179.
- [6] R.E. Morris, R.E. Aird, P. del Socorro Murdoch, H. Chen, J. Cummings, N.D. Hughes, S. Parsons, A. Parkin, G. Boyd, D.I. Jodrell, Inhibition of cancer cell growth by ruthenium(II) arene complexes, *Journal of Medicinal Chemistry* 44 (22) (2001) 3616–3621.
- [7] A. Habtemariam, M. Melchart, R. Fernández, S. Parsons, I.D. Oswald, A. Parkin, F.P. Fabbiani, J.E. Davidson, A. Dawson, R.E. Aird, Structure–activity relationships for cytotoxic ruthenium (II) arene complexes containing N,N-, N,O-, and O,O-chelating ligands, *Journal of Medicinal Chemistry* 49 (23) (2006) 6858–6868.
- [8] C. Bolm, J. Gladysz, Introduction: enantioselective catalysis, *Chemical Reviews* 103 (2003) 2761–2762.
- [9] A. Modzelewska, C. Pettit, G. Achanta, N.E. Davidson, P. Huang, S.R. Khan, Anticancer activities of novel chalcone and bis-chalcone derivatives, *Bioorganic & Medicinal Chemistry* 14 (10) (2006) 3491–3495.
- [10] M. Liu, P. Wilairat, S.L. Croft, A.L.-C. Tan, M.-L. Go, Structure–activity relationships of antileishmanial and antimalarial chalcones, *Bioorganic & Medicinal Chemistry* 11 (13) (2003) 2729–2738.
- [11] Y.-M. Lin, Y. Zhou, M.T. Flavin, L.-M. Zhou, W. Nie, F.-C. Chen, Chalcones and flavonoids as anti-tuberculosis agents, *Bioorganic & Medicinal Chemistry* 10 (8) (2002) 2795–2802.
- [12] D.K. Mahapatra, S.K. Bharti, Therapeutic potential of chalcones as cardiovascular agents, *Life Sciences* 148 (2016) 154–172.
- [13] M. Muthukumar, P. Viswanathamurthi, Synthesis, characterization and catalytic studies of ruthenium (II) chalconate complexes, *Applied Organometallic Chemistry* 23 (2) (2009) 78–85.
- [14] R. Gaur, R.A. Khan, S. Tabassum, P. Shah, M.I. Siddiqi, L. Mishra, Interaction of a ruthenium (II)-chalcone complex with double stranded DNA: spectroscopic, molecular docking and nuclease properties, *Journal of Photochemistry and Photobiology A: Chemistry* 220 (2–3) (2011) 145–152.
- [15] R. Prajapati, S.K. Dubey, R. Gaur, R.K. Koiri, B.K. Maurya, S.K. Trigun, L. Mishra, Structural characterization and cytotoxicity studies of ruthenium (II)-dmsO-chloro complexes of chalcone and flavone derivatives, *Polyhedron* 29 (3) (2010) 1055–1061.
- [16] K.K. Jovanovic, N. Gligorijevic, R. Gaur, L. Mishra, S. Radulovic, Anticancer activity of two ruthenium (II)-DMSO-chalcone complexes: Comparison of cytotoxic, pro-apoptotic and antimetastatic potential, *J BUON* 21 (2) (2016) 482–490.
- [17] J. Pitchaimani, M.R.C. Raja, S. Sujatha, S.K. Mahapatra, D. Moon, S.P. Anthony, V. Madhu, Arene ruthenium (II) complexes with chalcone, aminoantipyrine and aminopyrimidine based ligands: synthesis, structure and preliminary evaluation of anti-leukemia activity, *RSC Advances* 6 (93) (2016) 90982–90992.
- [18] E. Alessio, L. Messori, NAMI-A and KP1019/1339, two iconic ruthenium anticancer drug candidates face-to-face: a case study in medicinal inorganic chemistry, *Molecules* 24 (10) (2019) 1995.
- [19] M. Groessl, E. Reisner, C.G. Hartinger, R. Eichinger, O. Semenova, A.R. Timerbaev, M.A. Jakupec, V.B. Arion, B.K. Keppler, Structure–activity relationships for NAMI-A-type complexes (HL)[trans-RuCl₄(S-dmsO) ruthenate (III)](L= imidazole, indazole, 1, 2, 4-triazole, 4-amino-1, 2, 4-triazole, and 1-methyl-1, 2, 4-triazole): Aquation, redox properties, protein binding, and antiproliferative activity, *Journal of Medicinal Chemistry* 50 (9) (2007) 2185–2193.
- [20] A. Casini, C. Gabbiani, F. Sorrentino, M.P. Rigobello, A. Bindoli, T.J. Geldbach, A. Marrone, N. Re, C.G. Hartinger, P.J. Dyson, Emerging protein targets for anticancer metallodrugs: inhibition of thioredoxin reductase and cathepsin B by antitumor ruthenium (II)–arene compounds, *Journal of Medicinal Chemistry* 51 (21) (2008) 6773–6781.
- [21] J.P. Coverdale, T. Laroia-McCarron, I. Romero-Canelón, Designing ruthenium anticancer drugs: what have we learnt from the key drug candidates? *Inorganics* 7 (3) (2019) 31.
- [22] A. Bergamo, G. Sava, Ruthenium anticancer compounds: myths and realities of the emerging metal-based drugs, *Dalton Transactions* 40 (31) (2011) 7817–7823.
- [23] A. Bergamo, A. Masi, A. Peacock, A. Habtemariam, P.J. Sadler, G. Sava, In vivo tumour and metastasis reduction and in vitro effects on invasion assays of the ruthenium RM175 and osmium AFAP51 organometallics in the mammary cancer model, *Journal of Inorganic Biochemistry* 104 (1) (2010) 79–86.
- [24] A. Weiss, R.H. Berndsen, M. Dubois, C. Müller, R. Schibli, A.W. Griffioen, P.J. Dyson, P. Nowak-Sliwinska, In vivo anti-tumor activity of the organometallic ruthenium(II)-arene complex [Ru(η^6 -p-cymene)Cl₂(pta)](RAPTA-C) in human ovarian and colorectal carcinomas, *Chemical Science* 5 (12) (2014) 4742–4748.
- [25] G. Devagi, F. Dallemer, P. Kalaivani, R. Prabhakaran, Organometallic ruthenium(II) complexes containing NS donor Schiff bases: Synthesis, structure, electrochemistry, DNA/BSA binding, DNA cleavage, radical scavenging and antibacterial activities, *Journal of Organometallic Chemistry* 854 (2018) 1–14.
- [26] M. Ganeshpandian, R. Loganathan, E. Suresh, A. Riyasdeen, M.A. Akbarsha, M. Palaniandavar, New ruthenium (II) arene complexes of anthracenyl-appended diazacycloalkanes: effect of ligand intercalation and hydrophobicity on DNA and protein binding and cleavage and cytotoxicity, *Dalton Transactions* 43 (3) (2014) 1203–1219.
- [27] T. Khamrang, R. Kartikeyan, M. Velusamy, V. Rajendiran, R. Dhivya, B. Perumalsamy, M.A. Akbarsha, M. Palaniandavar, Synthesis, structures, and DNA and protein binding of ruthenium (II)-p-cymene complexes of substituted pyridylimidazo[1,5-a]pyridine: enhanced cytotoxicity of complexes of ligands appended with a carbazole moiety, *RSC Advances* 6 (115) (2016) 114143–114158.
- [28] W. Guo, W. Zheng, Q. Luo, X. Li, Y. Zhao, S. Xiong, F. Wang, Transferrin serves as a mediator to deliver organometallic ruthenium(II) anticancer complexes into cells, *Inorganic Chemistry* 52 (9) (2013) 5328–5338.
- [29] L. Colina-Vegas, W. Villarreal, M. Navarro, C.R. de Oliveira, A.E. Graminha, P.L.d.S. Maia, V.M. Deflon, A.G. Ferreira, M.R. Cominetti, A.A. Batista, Cytotoxicity of Ru(II) piano-stool complexes with chloroquine and chelating ligands against breast and lung tumor cells: Interactions with DNA and BSA, *Journal of Inorganic Biochemistry* 153 (2015) 150–161.
- [30] M. Ganeshpandian, M. Palaniandavar, A. Muruganatham, S.K. Ghosh, A. Riyasdeen, M.A. Akbarsha, Ruthenium (II)-arene complexes of diimines: Effect of diimine intercalation and hydrophobicity on DNA and protein binding and cytotoxicity, *Applied Organometallic Chemistry* 32 (3) (2018) e4154.
- [31] M. Bennett, T.N. Huang, T. Matheson, A. Smith, S. Ittel, W. Nickerson, 16(η^6 -Hexamethylbenzene) Ruthenium Complexes, *Inorganic Syntheses* 21 (1982) 74–78.
- [32] A. Kurzwernhart, W. Kandiolter, S. Bächler, C. Bartel, S. Martic, M. Buczkowska, G. Mühlgassner, M.A. Jakupec, H.-B. Kraatz, P.J. Bednarski, Structure–activity relationships of targeted Ru(II)-p-cymene anticancer complexes with flavonol-derived ligands, *Journal of Medicinal Chemistry* 55 (23) (2012) 10512–10522.
- [33] CrysAlis CCD, Oxford Diffraction Ltd., Version 1.171.32.29 (release 10-02008 CrysAlis171.NET).
- [34] M.C. Burla, R. Caliendo, B. Carrozzini, G.L. Cascarano, C. Cuocci, C. Giacovazzo, M. Mallamo, A. Mazzzone, G. Polidori, Crystal structure determination and refinement via SIR2014, *Journal of Applied Crystallography* 48 (1) (2015) 306–309.
- [35] G. Sheldrick, SHELXL-97, Program for the Refinement of Crystal Structures, University of Göttingen, Göttingen, Germany, 1997.
- [36] C.F. Macrae, I.J. Bruno, J.A. Chisholm, P.R. Edgington, P. McCabe, E. Pidcock, L. Rodriguez-Monge, R. Taylor, J. Streek, P.A. Wood, Mercury CSD 2.0—new features for the visualization and investigation of crystal structures, *Journal of Applied Crystallography* 41 (2) (2008) 466–470.
- [37] A.L. Spek, Structure validation in chemical crystallography, *Acta Crystallographica Section D: Biological Crystallography* 65 (2) (2009) 148–155.
- [38] L.J. Farrugia, WinGX suite for small-molecule single-crystal crystallography, *Journal of Applied Crystallography* 32 (4) (1999) 837–838.
- [39] CrysAlisPro 1.171.38.43 (Rigaku Oxford Diffraction) Empirical absorption correction using spherical harmonics, implemented in SCALE3 ABSPACK scaling algorithm, 2015.
- [40] E.B. Bauer, Chiral-at-metal complexes and their catalytic applications in organic synthesis, *Chemical Society Reviews* 41 (8) (2012) 3153–3167.
- [41] J. Wilmschurst, H. Bernstein, T. The vibrational spectra of pyridine, pyridine-4-d, pyridine-2,6-d₂, and pyridine-3,5-d₂, *Canadian Journal of Chemistry* 35 (10) (1957) 1183–1194.
- [42] K.N. Wong, S.D. Colson, The FT-IR spectra of pyridine and pyridine-d₅, *Journal of Molecular Spectroscopy* 104 (1) (1984) 129–151.
- [43] L. Corrin, B.J. Fax, R.C. Lord, The Vibrational Spectra of Pyridine and Pyridine-d₅, *The Journal of Chemical Physics* 21 (7) (1953) 1170–1176.
- [44] F.P. Urena, M.F. Gomez, J.L. González, E.M.n. Torres, A new insight into the vibrational analysis of pyridine, *Spectrochimica Acta Part A: Molecular and Biomolecular Spectroscopy* 59 (12) (2003) 2815–2839.
- [45] K. Nakamoto, Infrared spectra of inorganic and coordination compounds, Wiley Interscience, New York, 1970.
- [46] R. Gaur, L. Mishra, Synthesis and characterization of Ru (II)-DMSO-Cl-chalcone complexes: DNA binding, nuclease, and topoisomerase II inhibitory activity, *Inorganic Chemistry* 51 (5) (2012) 3059–3070.
- [47] P. Viswanathamurthi, M. Muthukumar, Ruthenium (II) carbonyl complexes containing chalconates and triphenylphosphine/arsine, *Journal of Chemical Sciences* 123 (5) (2011) 567–576.
- [48] M. Muthukumar, P. Viswanathamurthi, Spectral, catalytic, and antifungal studies of ruthenium (II) chalcone complexes, *Journal of Coordination Chemistry* 63 (7) (2010) 1263–1272.
- [49] I. Turel, J. Kljun, F. Perdih, E. Morozova, V. Bakulev, N. Kasyanenko, J.A.W. Byl, N. Osheroff, First ruthenium organometallic complex of antibacterial agent ofloxacin. Crystal structure and interactions with DNA, *Inorganic Chemistry* 49 (23) (2010) 10750–10752.
- [50] O. Novakova, H. Chen, O. Vrana, A. Rodger, P.J. Sadler, V. Brabec, DNA interactions of monofunctional organometallic ruthenium (II) antitumor complexes in cell-free media, *Biochemistry* 42 (39) (2003) 11544–11554.
- [51] R.A. Khan, F. Arjmand, S. Tabassum, M. Monari, F. Marchetti, C. Pettinari, Organometallic ruthenium (II) scorpionate as topo II α inhibitor; in vitro bind-

- ing studies with DNA, HPLC analysis and its anticancer activity, *Journal of Organometallic Chemistry* 771 (2014) 47–58.
- [52] S. Despax, F. Jia, M. Pfeffer, P. Hébraud, Complexation of DNA with ruthenium organometallic compounds: the high complexation ratio limit, *Physical Chemistry Chemical Physics* 16 (22) (2014) 10491–10502.
- [53] V. Marković, N. Debeljak, T. Stanojković, B. Kolundžija, D. Sladić, M. Vujčić, B. Janović, N. Tanić, M. Perović, V. Tešić, Anthraquinone–chalcone hybrids: synthesis, preliminary antiproliferative evaluation and DNA–interaction studies, *European Journal of Medicinal Chemistry* 89 (2015) 401–410.
- [54] X. Zarate, E. Schott, C.A. Escobar, R. Lopez-Castro, C. Echeverria, L. Alvarado-Soto, R. Ramirez-Tagle, Interaction of chalcones with ct-dna by spectrophotometric analysis and theoreticalsimulations, *Química Nova* 39 (8) (2016) 914–918.
- [55] A. Zahirović, D. Žilić, S.K. Pavelić, M. Hukić, S. Muratović, A. Harej, E. Kahrović, Type of complex–BSA binding forces affected by different coordination modes of alliin in novel water-soluble ruthenium complexes, *New Journal of Chemistry* 43 (15) (2019) 5791–5804.
- [56] Q. Xiao, S. Huang, Y. Liu, F.-F. Tian, J.-C. Zhu, Thermodynamics, conformation and active sites of the binding of Zn–Nd hetero-bimetallic Schiff base to bovine serum albumin, *Journal of Fluorescence* 19 (2) (2009) 317.
- [57] L.S. de Barros, O.A. Chaves, E. Schaeffer, C.M.R. Sant’Anna, A.B. Ferreira, D. Cesarin-Sobrinho, F.A. da Silva, J.C. Netto-Ferreira, Evaluating the interaction between di-fluorinated chalcones and plasmatic albumin, *Journal of Fluorine Chemistry* 190 (2016) 81–88.
- [58] K.M. Naik, S.T. Nandibewoor, Spectroscopic studies on the interaction between chalcone and bovine serum albumin, *Journal of Luminescence* 143 (2013) 484–491.
- [59] T.A. Khan, K. Bhar, R. Thirumoorthi, T.K. Roy, A.K. Sharma, Design, synthesis, characterization and evaluation of the anticancer activity of water-soluble half-sandwich ruthenium (ii) arene halido complexes, *New Journal of Chemistry* 44 (1) (2020) 239–257.
- [60] P. Sathyadevi, P. Krishnamoorthy, N.S. Bhuvanesh, P. Kalaiselvi, V.V. Padma, N. Dharmaraj, Organometallic ruthenium (II) complexes: Synthesis, structure and influence of substitution at azomethine carbon towards DNA/BSA binding, radical scavenging and cytotoxicity, *European Journal of Medicinal Chemistry* 55 (2012) 420–431.
- [61] P.K. Yaman, B. Şen, C.S. Karagöz, E. Subaşı, Half-sandwich ruthenium-arene complexes with thiophen containing thiosemicarbazones: Synthesis and structural characterization, *Journal of Organometallic Chemistry* 832 (2017) 27–35.
- [62] B. Demoro, R.F. De Almeida, F. Marques, C.P. Matos, L. Otero, J.C. Pessoa, I. Santos, A. Rodríguez, V. Moreno, J. Lorenzo, Screening organometallic binuclear thiosemicarbazone ruthenium complexes as potential anti-tumour agents: cytotoxic activity and human serum albumin binding mechanism, *Dalton Transactions* 42 (19) (2013) 7131–7146.
- [63] T.S. Kamatchi, P. Kalaivani, P. Poornima, V.V. Padma, F.R. Fronczek, K. Nataraajan, New organometallic ruthenium (II) complexes containing chelidonic acid (4-oxo-4 H-pyran-2, 6-dicarboxylic acid): synthesis, structure and in vitro biological activity, *RSC Advances* 4 (4) (2014) 2004–2022.
- [64] D. İnci, R. Aydın, Ö. Vatan, T. Sevgi, D. Yılmaz, Y. Zorlu, Y. Yerli, B. Çoşut, E. Demirkan, N. Çinkılıç, Synthesis and crystal structures of novel copper (II) complexes with glycine and substituted phenanthrolines: reactivity towards DNA/BSA and in vitro cytotoxic and antimicrobial evaluation, *JBIC Journal of Biological Inorganic Chemistry* 22 (1) (2017) 61–85.
- [65] B. Russell, K. Kubiak-Ossowska, P. Mulheran, D. Birch, Y. Chen, Locating the nucleation sites for protein encapsulated gold nanoclusters: a molecular dynamics and fluorescence study, *Physical Chemistry Chemical Physics* 17 (34) (2015) 21935–21941.
- [66] M. Shahid, H.M. Chawla, Dansylated adenine as a molecular probe for exploring hydrophobic pocket of bovine serum albumin (BSA) and its utility for mercury ion recognition, *Journal of Luminescence* 188 (2017) 460–464.